Research Square

Preprints are preliminary reports that have not undergone peer review.
They should not be considered conclusive, used to inform clinical practice,
or referenced by the media as validated information.

Glucose-xylose co-utilization and lactate production with engineered thermophilic Parageobacillus thermoglucosidasius

Panagiotis Kopsiaftis
Corbion (Netherlands)
Mats Meulemans
Wageningen University & Research
Jelmar de Vries
Wageningen University & Research
Christina Ludwig
Technical University of Munich
Harald J. Ruijssenaars
Corbion (Netherlands)
Nico J. Claassens
nico.claassens@wur.nl
Wageningen University & Research
Richard van Kranenburg
Wageningen University & Research

Research Article

Keywords:

Posted Date: October 7th, 2026

DOI: https://doi.org/10.21203/rs.3.rs-10242303/v1

License: This work is licensed under a Creative Commons Attribution 4.0 International License.
Read Full License

Additional Declarations: No competing interests reported.

Abstract

Background

Lignocellulose is a renewable feedstock rich in glucose and xylose, yet most microbes preferentially prioritize the consumption of glucose due to carbon catabolite repression (CCR), which can limit titers and productivity in bioprocesses. In this study, we employed a reverse engineering approach based on a previous adaptive laboratory evolution (ALE) investigation to construct and study *Parageobacillus thermoglucosidasius* DSM 2542 mutants capable of glucose-xylose co-utilization. Additionally, we rationally engineered xylose uptake and utilization by introducing derepressed operons related to the xylose assimilation pathway.

Results

To tackle CCR in *P. thermoglucosidasius*, we introduced a single nucleotide mutation resulting in an amino-acid substitution in PtsG, a component of the glucose phosphotransferase uptake system, and knocked-out the ribose operon repressor (*rbsR*). Mutant strains *ptsG*R452C, Δ*rbsR* and *ptsG*R452C Δ*rbsR* exhibited improved glucose-xylose co-utilization under microaerobic conditions, which was accompanied by the derepression of multiple operons typically governed by carbon catabolite repression (CCR), as suggested by proteome analysis. Next to the reverse engineering approach, we rationally engineered xylose metabolism, too. Promoter activity studies of the native xylose utilization operon (*xylAB*) and a xylose transporter (*xylFGH*) indicated regulation by both CCR, and xylose induction. Constitutive expression of *xylAB* and a CCR-unresponsive *xylFGH* mutant under the P_{ldhL} promoter resulted in faster growth on xylose-containing media. Last, the strains developed in this study were cultivated in bioreactors and evaluated for their glucose-xylose utilization and lactate production. Mutants *ptsG*R452C, Δ*rbsR* and *ptsG*R452C Δ*rbsR* showed a clear phenotype of reduced CCR, whereas *xylAB* overexpression improved xylose consumption in the presence of glucose notably leading to almost complete consumption of xylose in mixed-sugar fermentations. WT achieved a lactate yield of 56.76 mol-% on the glucose-xylose mixed substrate, whereas mutants Δ*rbsR* and P_{ldhL}-*xylAB* exhibited the highest values, reaching 73 mol-% and 63 mol-%, respectively.

Conclusions

In summary, carbon catabolite repression in *Parageobacillus thermoglucosidasius* was addressed through rational and reverse engineering strategies. Constitutive expression of derepressed *xylAB* and *xylFGH* improved xylose utilization, yet did not fully remove CCR. Reverse-engineered ALE-derived mutations in *ptsG* and *rbsR* facilitated glucose-xylose co-utilization. Bioreactor studies demonstrated that multiple strains could achieve higher lactate yield compared to the WT.

INTRODUCTION

Bio-based production processes mostly rely on first generation feedstocks such as can sugar and corn dextrose (Lennartsson et al., 2014), with production of lactate and amino acids being some of the most representative examples in the bioprocessing field. Yet, concerns about the use of such crops often center on their life-cycle greenhouse gas emissions, environmental degradation and low energy returns on investment (Hill, 2022). On the other hand, second generation feedstocks are non-food biomasses derived from agricultural or logging activities in the form of waste (Mohr and Raman, 2013). Despite the widespread availability of lignocellulosic biomass, its commercial use remains limited (Broda et al., 2022), with Raizen's Brazilian bioethanol facility representing the only commercial lignocellulosic biorefinery currently in operation. While lignocellulose represents a critical feedstock for advancing the circular bioeconomy (Francois et al., 2020), its valorization is constrained by the inherent recalcitrance of the biomass, logistics and the technical challenges associated with efficient upstream as well as downstream processing.

Lignocellulose is a principal component of the plant cell wall and is composed of three polymers: cellulose, hemicellulose, and lignin (Singhvi and Gokhale, 2019). Unlike lignin, cellulose and hemicellulose can be a source for fermentable sugars for bioproduction. Cellulose is a homopolymer of glucose, whereas hemicellulose is a heteropolymer, which predominantly contains xylose, often decorated with arabinose, galactose, and glucuronic acid (Singhvi and Gokhale, 2019). Industrial bioconversion of lignocellulose often relies on Separate Hydrolysis and Fermentation (SHF) (Devi et al., 2022) or Simultaneous Saccharification and Fermentation (SSF) (Olofsson et al., 2008). Both processes rely on degradation of the lignocellulosic biomass by specific glycoside hydrolases (Álvarez et al., 2016). In SHF, the hydrolysis of lignocellulose is decoupled from the fermentation process, while in SSF hydrolysis and fermentation occur in the same step. Specifically, in an SHF configuration, hydrolysis is first performed at elevated temperatures (typically 50–55°C at reduced pH) to maximize enzymatic activity. The resulting hydrolysate, rich in sugars, is subsequently fermented by microbial cells after lowering the temperature to suit microbial growth (Devi et al., 2022). Conversely, SSF allows hydrolysis and fermentation to occur simultaneously, where the substrate, enzymes, and microbial cells interact in parallel to degrade the polymers and subsequently consume the released sugars.

Although mesophilic microorganisms such as *Saccharomyces cerevisiae* (Cunha et al., 2018) often present the conventional choice for lignocellulose bioconversion, their implementation in SSF is limited by the mismatch between their optimal growth temperature, and the elevated temperatures preferred for enzymatic biomass hydrolysis. Hence, it was suggested before that lignocellulose bioprocessing may benefit from the use of thermophilic microbes, which can grow at temperatures similar to those allowing optimal activity of the hydrolytic enzymes, better facilitating SSF or SHF without the need for cooling in between hydrolysis and fermentation (Ibrahim et al., 2017; Turner et al., 2007). Moreover, effective SHF and SSF implementation requires the use of microbes capable of growing on both C_6 and C_5 sugars, especially glucose and xylose, which are predominantly present in the hydrolysate of lignocellulose.

Consequently, microbes that can co-utilize these sugars while growing at elevated temperatures represent attractive platforms for developing chassis relevant to lignocellulose bioprocessing.

Parageobacillus thermoglucosidasius is a Gram-positive and facultative anaerobic bacterium that exhibits the abovementioned preferable traits as it grows optimally at 60–65°C (Hussein et al., 2015) and can utilize both glucose and xylose (Suzuki et al., 1983). Various studies have focused on engineering *P. thermoglucosidasius* for effective production of metabolites such as lactate (van Kranenburg et al., 2017), ethanol (Cripps et al., 2009; Calverley et al., 2024), isobutanol (Lin et al., 2014) and riboflavin (Wang et al., 2022, Wang et al., 2024). *P. thermoglucosidasius* in mixed-sugar cultivations first consumes glucose, then xylose, due to Carbon Catabolite Repression (CCR) (Liang et al., 2022[a]). Sequential sugar use reduces productivity, slows xylose utilization, and extends fermentation time (Kim et al., 2010; Vinuselvi et al., 2012). Therefore, eliminating CCR may improve the efficiency of lignocellulose-based bioproduction processes. CCR in *Bacillus subtilis*, a model organism for Gram-positive bacteria, is well-studied (Fujita et al., 2009; Görke and Stülke, 2008) and serves as a valuable reference for understanding CCR in other Gram-positive bacteria, such as *P. thermoglucosidasius*. The signal transduction pathway in *B. subtilis* and *P. thermoglucosidasius* starts with the simultaneous uptake and phosphorylation of glucose from the phosphotransferase uptake system (PTS) (Bidart et al., 2023). Once glucose is simultaneously taken up and phosphorylated, it enters glycolysis leading to accumulation of fructose-1,6-biphosphate (FBP). FBP activates the Hpr kinase (HprK), which in turn phosphorylates Hpr on the Ser46 residue. The Hpr-Ser46-P binds to the master regulator CcpA and to less extent to Crh (Landmann, et al., 2011; Galinier et al., 1997), and the complex CcpA-Hpr-Ser46-P or Crh-Hpr-Ser46-P binds to nucleotide sequences named catabolite responsive elements (*cre*), which are located either upstream or within coding sequences, thereby repressing the expression of these genes. Carbon catabolite repression (CCR) commonly targets genes involved in the utilization of less preferred sugars, such as xylose and arabinose. CCR provides a competitive advantage in natural environments by prioritizing carbon sources that support rapid growth, thereby minimizing unnecessary protein synthesis (Görke and Stülke, 2008). Glucose is strongly preferred over xylose because its uptake and phosphorylation are coupled through the phosphotransferase system (PTS), consuming a single phosphoenolpyruvate (PEP) molecule, *de facto* requiring net 1 ATP equivalent. In contrast, xylose uptake and conversion to glycolytic intermediates require a net investment of two ATP equivalents. Specifically, xylose is imported via ABC transporters at the cost of one ATP and subsequently phosphorylated by xylose kinase, consuming an additional ATP. Furthermore, phosphorylated glucose directly enters the Embden-Meyerhof-Parnas (EMP) pathway, whereas xylose must first undergo multiple rearrangement steps through the pentose phosphate pathway before feeding into central metabolism. Together, the lower initial energy investment and more direct entry into the EMP pathway allow higher maximum specific growth rates to be achieved on glucose compared to xylose (Gonzalez et al., 2018), and can explain the preferential consumption of glucose over xylose.

To tackle CCR, Liang et al., (2022[b]) adopted an adaptive laboratory evolution (ALE) strategy to develop *P. thermoglucosidasius* strains capable of simultaneous glucose and xylose utilization. Genomic

characterization of the evolved strains revealed multiple mutations, several of which were directly involved in carbon metabolism. Notably, the evolved strain harbored an amino acid substitution (R452C) in the PtsG component of the glucose-specific phosphotransferase system (PTS), which functions as a transmembrane glucose transporter responsible for the uptake and immediate phosphorylation of glucose. Additionally, the evolved strain carried a frameshift mutation in the ribose operon repressor gene (*rbsR*). These genetic alterations were hypothesized to have significantly altered the sugar uptake kinetics and regulatory profile of the adapted phenotype. The PtsGR452C may have resulted in reduced glucose uptake potentially leading to reduced CcpA-exerted repression, whereas the loss of the RbsR function may have led to constitutive expression of the ribose ABC transporter, which could promiscuously import xylose, too. Altogether, the co-existence of these mutations may have enabled *P. thermoglucosidasius* to metabolize xylose in the presence of glucose.

P. thermoglucosidasius DSM 2542 assimilates xylose via the xylose isomerase (XylA) and xylulose kinase (XylB) encoded by the *xylAB* operon. This strain has no specifically annotated xylose transporter, however xylose import has been suggested to be coordinated via multiple sugar transporters including the ribose ABC transporter, the arabinose ABC transporter, and unknown sugar ABC transporters (Liang et al., 2022[a,b]). Moreover, a recent study identified an ABC transporter that could also potentially import xylose (Wang et al., 2024). The transcriptional control of the xylose-specific transport and catabolic operons are probably subject to a dual regulatory mechanism: repression by the xylose-responsive regulator XylR, in the absence of xylose, and CCR by CcpA, in the presence of glucose as indicated by Wang et al., (2024). As demonstrated in previous studies (Liang et al., 2022[a]), *P. thermoglucosidasius* DSM 2542 exhibits a relaxed form of catabolite repression including some xylose assimilation in the presence of glucose unlike other more strict examples of CCR (Liang et al., 2022[a]). Still there is reduced xylose utilization during growth on glucose, as well as following glucose depletion, possibly attributed to the time required to alleviate CcpA repression and fully induce the xylose assimilation pathways. Consequently, overcoming these regulatory bottlenecks is a critical prerequisite for achieving the high volumetric productivities required for economically viable lignocellulosic biorefineries.

In this study, we applied a reverse engineering approach to systematically reconstruct some of the mutations of the evolved strains. We also investigated the effect of glucose and xylose on both the native xylose utilization operon, and a xylose transporter operon from another related *P. thermoglucosidasius* strain. In parallel, we implemented the previously reported mutations in *ptsG* and *rbsR* - both individually and in combination - allowing co-consumption of glucose and xylose in *P. thermoglucosidasius*, which was further validated by comparative proteomic analysis revealing distinct differences between the mutant and wild-type strains. Additionally, we sought to enhance specific growth rates on xylose by overexpressing the native xylose assimilation operon *xylAB* and a xylose-specific transporter *xylFGH* across both wild-type and mutant genetic backgrounds. Finally, the engineered strains were cultivated in bench-scale bioreactors to assess glucose-xylose consumption and lactate production.

MATERIALS AND METHODS

General cultivation techniques, media composition, bacterial strains, and plasmids.

For the cultivation of *E. coli* strains, lysogeny broth (LB) medium was used containing 10 g/L tryptone (BactoTM), 10 g/L NaCl, and 5 g/L yeast extract (BactoTM). Solid LB medium additionally contained 15 g/L agar. *E. coli* strains used in molecular cloning of pNW33n or pMM7 plasmid vectors were cultivated in 10 mL liquid medium in falcon tubes at 37°C and 200 rpm overnight or on solid medium at 37°C overnight, while temperature was set to 30°C for *E. coli* strains used in molecular cloning of pUCG3.8 plasmid vectors.

For general cultivation, *P. thermoglucosidasius* strains were cultivated in TGP liquid medium containing 17 g/L tryptone (BactoTM), 3 g/L peptone (Sigma Aldrich), 5 g/L NaCl, 2.5 g/L K_2HPO_4, 0.4% (w/v) glycerol, and 4 g/L sodium pyruvate or on solid TSA (Millipore) medium. For the experimental investigation of growth in glucose and xylose mixes, *P. thermoglucosidasius* was cultivated in thermophilic minimal media (TMM). TMM contained: 494 mg/L NaCl, 145 mg/L $NaSO_4$, 24.7 mg/L KCl, 3.97 mg/L KBr, 184 mg/L $MgCl_2 \cdot 6\ H_2O$, 89.2 mg/L $NaNO_3$, 8.37 g/L MOPS, 3.58 mg/L $FeSO_4$, 716 mg/L tricine, 229 mg/L K_2HPO_4, 0.51 g/L NH_4Cl, 73.5 mg/L $CaCl_2$, 2 µg/L biotin, 5 µg/L thiamine-HCl, 2 µg/L folic acid, 0.1ug/L vitamin B_{12}, 0.127 µg/L spermidine, 174 µg/L spermine tetrahydrochloride, 0.7 mg/L hemin, 1 mg/L $FeCl_3 \cdot 6\ H_2O$, 0.18 mg/L $ZnSO_4 \cdot 7\ H_2O$, 0.12 mg/L $CuCl_2 \cdot 2\ H_2O$, 0.12 mg/L, $MnSO_4 \cdot\ H_2O$, and 0.18 mg/L $CoCl_2 \cdot 6\ H_2O$, with a variable carbon source. Glucose, xylose or both glucose and xylose were added as carbon source to concentrations as specified in the Results section.

When needed for cloning, plasmid propagation or cultivation, chloramphenicol (15 µg/L) or kanamycin (25 µg/L) was added to *E. coli* cultures, while either chloramphenicol (8 µg/L) or kanamycin (12.5 µg/L) was added to *P. thermoglucosidasius* cultures.

Plasmid assembly and genome modification

Generally, primers (Table S1) were designed to provide homology for Gibson assembly or for introducing SacI/KpnI restriction enzyme recognition sites. All the desired DNA fragments were amplified using Q5 polymerase (Q5 2x MasterMix, NEB), isolated from a 1% agarose gel (Zymogen gel DNA recovery kit) and assembled by either Gibson HiFi assembly (NEB, 50°C, 30 minutes) or T4 DNA Ligation reactions (NEB, 15°C, 16 hours). For pNW33n 1 µL of ligation or Gibson mixture was used to transform NEB10b chemically competent cells (NEB) by heat shock, while for pMM7 or pUCG3.8 based vectors 1 µL of ligation or Gibson mixture was transformed by electroporation in commercially electrocompetent cells ElectroMAX™ Stbl4™ (New England Biolabs). Plasmid presence in bacterial cells was verified by colony PCR using OneTaq polymerase (OneTaq 2x MM, New England Biolabs). Plasmids were isolated (QIAprep Spin Miniprep Kit, Qiagen) and the sequence of all newly assembled plasmids were confirmed by Oxford Nanopore whole plasmid sequencing (Plasmidsaurus).

Confirmed plasmids (Table 1) were used to transform electrocompetent *P. thermoglucosidasius* by electroporation, following a protocol described previously by Millgaard et al., (2023). To introduce the *ptsG*R452C mutation and knock-out *rbsR*, we induced homologous recombination with homology arms (upstream flank - US, downstream flank - DS) from pNW33n-US-*ptsG*R452C-DS or pNW33n-US-*rbsR*-DS onto the genome of a sporulation-deficient strain *P. thermoglucosidasius* DSM 2542 Δ*sigF* (van Kranenburg et al., 2017) and selected against wild-type DNA by using the protocol described previously by Millgaard et al., (2023). Colonies during the first recombination event or second recombination event were screened by colony PCR using OneTaq polymerase (OneTaq 2x MM, New England Biolabs). Mutants were confirmed after the second recombination event with Sanger sequencing, then cultivated overnight in TGP medium and stored in glycerol at -70°C.

Table 1
– List of plasmids used in this study

Name	Description	Source/Reference
pUCG3.8	*E. coli*/*Geobacillus* shuttle vector; *KanR*, pMB1 *ori*, *repBST1 ori*	Bartosiak-Jentys et al., 2013
pNW33n	*E. coli*/*Geobacillus* shuttle vector; *CamR*, pUC19 *ori*, pTHT15 *ori*	Bacillus Genetic Stock Center
pMM7	*E. coli*/*P. thermoglucosidasius* shuttle vector; Temp-sensitive *repB*, *ColE1*, *KanR*, *sfGFP*; contains *spo0A* deletion flanks	Millgaard et al., 2023
pUCG3.8-P_{ldhL}-*xylAB*	pUCG3.8-P_{ldhL}-RBS_{pheB}-*xylAB*-dbt terminator (overexpression of *xylAB*; dbt terminator sequence similar to Yang et al., 2023)	This study
pUCG3.8-P_{ldhL}-*xylFGH* (*cre*$^+$)	pUCG3.8-P_{ldhL}-RBS_{pheB}-*xylFGH* (overexpression of *xylFGH* with *cre*)	This study
pUCG3.8-P_{ldhL}-*xylFGH* (*cre*$^-$)	pUCG3.8-P_{ldhL}-RBS_{pheB}-*xylFGH* (overexpression of *xylFGH* without *cre*)	This study
pNW33n-US-*ptsG*R452C-DS	Plasmid containing the *ptsG*R452C CDS with 500 bp upstream and downstream flanks targeting the *ptsG*	This study
pMM7-US-*rbsR*-DS	Plasmid containing the 500 bp upstream and Downstream flanks targeting the *rbsR* for frameshift after the fifth codon	This study
pUCG3.8-P_{xylAB}-*sfGFP*	Plasmid expressing a variant of *sfGFP* under the control of the *xylAB* promoter and RBS	This study
pUCG3.8-P_{xylFGH}-*sfGFP*	Plasmid expressing a variant of *sfGFP* under the control of the TNO-09.020 *xylFGH* promoter and RBS	This study

Table 2
– List of strains used in this study

Name	Description	Source
E. coli Stbl4	*mcrA Δ(mcrBC-hsdRMS-mrr) recA1 endA1 gyrA96 gal– thi1 supE44 λ–relA1 Δ(lac-proAB) / F' [proAB+lacIqZΔM15 Tn10(TetR)]*	ThermoFisher
E. coli NEB10b	*Δ(ara-leu) 7697 araD139 fhuA ΔlacX74 galK16 galE15 e14- ϕ80dlacZΔM15 recA1 relA1 endA1 nupG rpsL (Str^R) rph spoT1 Δ(mrr-hsdRMS-mcrBC)*	NEB
WT	*P. thermoglucosidasius* DSM 2542 Δ*sigF*	van Kranenburg et al., 2017
P$_{ldhL}$-*xylAB*	*P. thermoglucosidasius* DSM 2542 Δ*sigF* pUCG3.8-P$_{ldhL}$-*xylAB*	This study
P$_{ldhL}$-*xylFGH*	*P. thermoglucosidasius* DSM 2542 Δ*sigF* pUCG3.8-P$_{ldhL}$-*xylFGH* (modified *cre* from *xylF* CDS)	This study
P$_{ldhL}$-*xylFGH* (*cre*$^+$)	*P. thermoglucosidasius* DSM 2542 Δ*sigF* pUCG3.8-P$_{ldhL}$-*xylFGH* (intact *cre* from *xylF* CDS)	This study
*ptsG*R452C	*P. thermoglucosidasius* DSM 2542 Δ*sigF ptsG*R452C (mutated *ptsG*)	This study
Δ*rbsR*	*P. thermoglucosidasius* DSM 2542 Δ*sigF* Δ*rbsR* (knocked-out *rbsR*)	This study
*ptsG*R452C Δ*rbsR*	*P. thermoglucosidasius* DSM 2542 Δ*sigF ptsG*R452C Δ*rbsR* (double mutant with mutated *ptsG* and knocked-out *rbsR)*	This study
*ptsG*R452C-pUCG3.8	*ptsG*R452C carrying an empty vector pUCG3.8	This study
*ptsG*R452C-P$_{ldhL}$-*xylAB*	*ptsG*R452C expressing *xylAB* operon	This study
*ptsG*R452C-P$_{ldhL}$-*xylFGH*	*ptsG*R452C expressing *xylFGH* operon	This study
P$_{xylAB}$-*sfGFP*	*P. thermoglucosidasius* DSM 2542 Δ*sigF* equipped with pUCG3.8-P$_{xylAB}$-*sfGFP*	This study
P$_{xylFGH}$-*sfGFP*	*P. thermoglucosidasius* DSM 2542 Δ*sigF* equipped with pUCG3.8-P$_{xylFGH}$-*sfGFP*	This study
ALE	*P. thermoglucosidasius* DSM 2542 2DG-ADE2	Liang et al., 2022[b]

Promoter characterization in plate reader

P. thermoglucosidasius harboring pUCG3.8, pUCG3.8-P_{xylAB}-sfGFP, or pUCG3.8-P_{xylFGH}-sfGFP were cultivated overnight in TGP liquid medium at 55°C. The next day, 200 µl of cells were centrifuged at 3000 x g for 3 min, and then washed twice with TMM (without carbon source). Supernatant was removed and cells were resuspended in TMM containing glucose 0.5% (w/v) or xylose 0.5% (w/v) or glucose 0.5% (w/v) and xylose 0.5% (w/v) supplemented together. For xylose titration xylose concentrations between 0.01% (w/v) and 1% (w/v) were added in TMM media. Resuspended cells were inoculated in a dark 96-well plate (flat bottom) in biological triplicates with media to a final OD_{600} of 0.1–0.2 and incubated in the BioTek Synergy Neo2 Reader (Agilent) at 57°C. The incubation protocol included OD_{600} and fluorescence measurement followed by 3 rounds of alternating 2 x 1 min linear and 2 x 1 min orbital shaking (total ~ 12 min per round of shaking). Fluorescence measurements were taken at wavelengths of 488 nm and 510 nm with gain = 80. The original *sfGFP* coding sequence as described by Frenzel et al., (2018) was mutated to remove a potential *cre* element. Its removal during molecular cloning resulted in two amino acid substitutions, specifically 148th and 203rd amino acids were substituted to Cysteine.

Tube cultivations

P. thermoglucosidasius strains were revived from glycerol stocks by growing in TGP liquid media at 60°C, unless if they carried a plasmid, then they were revived at 55°C. Following the overnight incubation, 1 mL of the cultures was transferred to 9 mL of fresh TGP and incubated further for 6–8 hours at 60°C or at 55°C, respectively. After the subculturing step, 1 mL of culture was centrifuged at 3000 x g for 3 min, washed with TMM broth (without carbon source), and the cell pellet was centrifuged and washed again. After the final wash step, cell pellet was resuspended in 1 mL of TMM containing 1% (w/v) glucose and 1% xylose (w/v). Duplicate conical-bottom tubes (15 mL) prefilled with TMM containing 1% (w/v) glucose and 1% xylose (w/v) were inoculated with resuspended cells to a starting OD_{600} = 0.1 and at a final working volume of 10 mL. 1 mL from each tube was sampled 24 hours after inoculation (or 36 hours if strains contained a plasmid) and supernatants were processed in HPLC for sugar quantification.

Fermenter cultivations

P. thermoglucosidasius strains were revived from glycerol stocks by growing on TGP liquid media at 60°C, unless if they carried a plasmid, then they were revived at 55°C. Following the overnight incubation, 5 mL of overnight culture was transferred to 45 mL TGP liquid media in 250 mL baffled flasks and incubated at 60°C, 200 rpm for approximately 6 hours. Following this subculturing step, the cultures were centrifuged at 3500 x g for 10 min, and washed twice with TMM broth (without carbon source). Final cell pellet was resuspended in 50 mL of TMM and was aseptically used to inoculate the bioreactors. Fermentations were performed in an Eppendorf DASGIP parallel bioreactor system equipped with glass reactors of 1.4 L and a working volume of 1 L. DASGIP control 4.0 was used to control the process. The fermentation conditions were as follows: temperature was controlled at 60°C, pH at 6.8 by addition of 3M KOH and the stirring speed was 200 rpm.

Calculations

Growth rates from microplate reader experiment were calculated using an algorithm of linear regression built in R studio. The detailed script is provided in the supplementary file. In brief, the script used a time window of 100 sampling times (approx. 1200 min total) to calculate the maximum specific growth rate, which fits the following requirements: a) at least 1.5 doubling times have occurred within this timeframe and b) the slope has an $R^2 > 0.8$. Significance for growth rates was done using ANOVA tests in which each mutant/media combination was compared to the respective WT/media combination. The following equations were used to estimate yield of lactate on substrate.

HPLC quantification of glucose, xylose and fermentation products

High Performance Liquid Chromatography (HPLC) was used to quantify glucose, xylose and fermentation products like lactate, acetate, formate and ethanol. Specifically, the DIONEX AS-AP instrument equipped with an Aminex-HPX-87H column running on 8 mM of H_2SO_4 mobile phase was used to detect glucose and xylose. A sample of 1 mL from the tube cultures or bioreactors was centrifuged at 21300 x g for 3 min and supernatant was temporarily stored at 4°C. 8 ul of the supernatant were mixed with 192 ul of 16 mM H_2SO_4. Samples were run at 0.2 mL/min flow rate and sugar peaks were detected using an RI and a UV detector. Initial results analyses for both types of HPLC was performed using the Chromeleon software.

Proteomic sample preparation

P. thermoglucosidasius WT, *ptsG*R452C, Δ*rbsR*, *ptsG*R452C Δ*rbsR* and ALE strains were inoculated from glycerol stocks in liquid TGP media and incubated overnight at 60°C, 200 rpm and were transferred the following day in fresh TGP media for 4–5 hours. After removing the preculture media by centrifugation (3500 x g, 10 minutes), 1 mL from each subculture was inoculated in eight 15 mL conical bottom screw cap tubes containing 9 mL of TMM supplemented with 1% (w/v) glucose and 1% (w/v) xylose. Cells were incubated at 60°C and 200 rpm, grown until OD_{600} = 0.5–0.7, then pooled in pairs of two to reach a volume of 20 mL liquid culture in quadruplicates, following harvest by centrifugation (4000 x g, 10 min), and storage at -20°C until further processing. Samples were processed for mass spectrometry according to a slightly modified version of the SPEED protocol (Abele et al., 2023; Doellinger et al., 2020). In brief, cells were resuspended in 100 µL 100% TFA and incubated in a thermocycler at 55°C. A volume of 900 µL 2 M Tris solution was added to neutralize the sample. The lysed samples were quantified by Bradford assay and stored at -70°C. A mass of 50 µg of protein per sample was reduced (10 mM TCEP) and carbamidomethylated (40 mM CAA) for five minutes at 95°C. Subsequently, the samples were diluted with water to achieve a final concentration of 1 M Tris and 5% TFA. The proteins were digested by adding trypsin (proteomics grade, Roche) at a 1/50 enzyme/protein ratio (w/w) and incubated at 37°C overnight. Digests were acidified by adding 3% (v/v) formic acid (FA) and desalted using self-packed StageTips

(five disks per micro-column, ø 1.5 mm, C18 material, 3 M Empore) (Rappsilber et al., 2007). The peptide eluates were dried to completeness and stored at − 80°C. Before mass spectrometric measurement, all samples were resuspended in 12 µl 0.1% FA in HPLC grade water and 5 µl were subjected to LC-MS/MS.

Proteomic data acquisition

Peptides were analyzed on a Vanquish Neo UHPLC (microflow configuration) coupled to an Orbitrap Exploris 480 mass spectrometer (both Thermo Fisher Scientific). Per sample, ca. 25 µg of peptides were applied onto a commercially available Acclaim PepMap 100 C18 column (2 µm particle size, 1 mm ID × 150 mm, 100 Å pore size; Thermo Fisher Scientific) and separated using a 60 min linear gradient ranging from 3% to 28% solvent B (0.1% FA, 3% DMSO in ACN) in solvent A (0.1% FA, 3% DMSO in HPLC grade water) at a flow rate of 50 µl/min. The mass spectrometer was operated in data-independent acquisition (DIA) mode. MS1 full scans (360–1300 m/z) were acquired with a resolution of 120,000, an absolute AGC target value of 1E6 and a maximum injection time of 50 ms. The cycle time was set to 3 seconds. MS2 scans (200–1800 m/z) were acquired over 40 DIA segments with widths adjusted to the precursor density. The MS2 scan resolution in the Orbitrap was set to 15,000 with an absolute AGC target value of 1E5 and a maximum injection time of 22 ms. The HCD collision energy was set to 30%.

Proteomic data analysis

The mass spectrometric raw files were analyzed with DIA-NN (version 1.8) (Demichev et al., 2020) using the NCBI *Parageobacillus thermoglucosidasius* protein database (GCF_001295365.1, downloaded January 2026) appended with common contaminants as well as ten mutated protein sequences to account for the mutated proteins occurred in the original ALE investigation (Liang et al., 2022[b]). FASTA digest for library-free search and deep learning-based spectra was enabled. N-term M excision, C carbamidomethylation, Ox(M), and Ac(N-term) were activated. The tryptic peptide length range was set from 7 to 30, precursor charge ranged from 2 to 6, precursor m/z ranged from 360 to 1300 and fragment ion m/z ranged from 200 to 1800. Usage of isotopologues and match-between runs (MBR) were enabled. Precursor FDR was set to 1%. All other parameters were kept as default.

The DIA-NN main report table “report.pg_matrix.tsv” and the herein included maxLFQ protein intensities were used to estimate differential protein abundance between conditions (Fig. 4, Figure S3). Significance was estimated using a Bonferroni test. To estimate protein mass fractions, the “report.pg_matrix.tsv” table was further processed with the R-script DIAgui (Gerault et al., 2024), to obtain “intensity based absolute quantification (iBAQ) values” (Figure S3 and S5). Further processing was carried out with the in-house proteomic analysis tool “baybiomsCruncher” (https://github.com/nava20ir/baybiomsCruncher) as well as excel. This included filtering proteins for being quantified in three out of four biological replicate measurements of at least one experimental condition. Missing values were imputed by replacement with random values drawn from a normal down-shifted distribution (width = 0.3, downshift = 1.8). The iBAQ protein intensities were normalized by median centering.

RESULTS

Mutating the ptsG and deleting rbsR affect growth of P. thermoglucosidasius in glucose and xylose

In a previous study by Liang et al. (2022[b]) the authors developed a *P. thermoglucosidasius* strain with alleviated CCR after multiple rounds of ALE in media containing xylose and a non-metabolizable analogue of glucose: 2-deoxy-glucose (2-DG). 2-DG can be imported by the PTS of *P. thermoglucosidasius*, however, further catabolism is arrested after phosphorylation to 2-DG-6P as it lacks the 2-OH group. This resulted in a selection pressure for xylose utilization in the presence of 2-DG. Genome sequencing of the mutant revealed multiple mutations of which only two mutations seem directly relevant to sugar utilization. Specifically, a single nucleotide mutation led to an amino acid substitution from arginine to cysteine in PtsG (R452C), the transmembrane component of the phosphotransferase uptake system responsible for the uptake and phosphorylation of glucose. Moreover, a frameshift mutation occurred knocking out the ribose operon repressor coding sequence (*rbsR*). To engineer a non-sporulating host platform harboring the abovementioned mutations and streamline laboratory handling, we employed a Δ*sigF* strain, which is a well-documented mutation for preventing sporulation (van Kranenburg et al., 2017). Specifically, we constructed three mutant strains of *P. thermoglucosidasius* DSM 2542 Δ*sigF* namely *ptsG*R452C, Δ*rbsR* and *ptsG*R452C Δ*rbsR* carrying the above mutations separately and in combination. All mutants were constructed using homologous recombination by employing plasmid vectors carrying homology arms for the sequences flanking the targeted genes.

The mutants constructed in this study, *i.e. ptsG*R452C, Δ*rbsR* and *ptsG*R452C Δ*rbsR* along with the WT and ALE strains, were first cultivated aerobically in minimal media to assess growth in the presence of 0.2% (w/v) glucose, 0.2% (w/v) xylose and co-presence of 0.2% (w/v) glucose and 0.2% (w/v) xylose. The growth rate in minimal media supplemented with glucose was only reduced for Δ*rbsR* and ALE (Fig. 1). Notable differences were observed in media with xylose; the *ptsG*R452C mutant exhibited significantly faster growth on xylose, whereas Δ*rbsR* showed impaired growth. Interestingly, all mutants outperformed WT when they were cultivated in mixed sugars both in growth rates and maximum biomass density achieved, however in all cases there was still some delayed second growth phase suggesting that in these aerobic conditions some CCR-like behavior is still present. Generally, the growth rates on xylose were significantly lower than on glucose, as expected.

Improving growth rates on xylose by overexpressing the native xylose assimilation pathway and a xylose ABC transporter

Xylose consumption in *P. thermoglucosidasius* DSM 2542 relies on xylose uptake and xylose assimilation intracellularly via XylA and XylB enzymes yielding xylulose-5P, which then enters the Pentose Phosphate Pathway (PPP). Xylose uptake in *P. thermoglucosidasius* DSM 2542 is mediated by multiple sugar transporters as it lacks a xylose-specific transporter (Liang et al., 2022[a]). Yet, Wang et al. (2024) recently proposed that the operon AOT_13435 - AOT_13445 encodes the primary ABC transporter responsible for

xylose uptake in *P. thermoglucosidasius* DSM 2542. This gene cluster is located adjacent to arabinose-utilization genes, approximately 30 kb away from the xylose assimilation genes *xylA* and *xylB*, and sequence analysis using BlastP (Figure S1) suggests that it may encode a more general monosaccharide transporter rather than a transporter with xylose-specific substrate preference. In our previous work (Paredes-Barrada et al., 2024), we examined coding regions relevant to sugar utilization within the Hemicellulose Utilization (HUS) locus across several *P. thermoglucosidasius* strains. This comparative analysis revealed that two *P. thermoglucosidasius* strains possess a more typical *xylFGH* transport operon. Specifically, the TNO-09.020 and BH4.1 strains encode an ABC transporter, which showed higher homology to established XylFGH xylose-specific transporters from *Escherichia coli* (NP_418023.1, NP_418025.1, NP_418024.1) and *Thermoanaerobacter ethanolicus* (AAC38794.1, Q6VMN4.1, WP_003870809.1) compared to the one present in DSM 2542 (Fig. 2). This suggests that xylose uptake mechanisms may differ between *P. thermoglucosidasius* strains and that the transporter present in the HUS locus of DSM 2542 may not represent the universally conserved xylose transporter in this species.

To improve xylose utilization and uptake in *P. thermoglucosidasius* DSM 2542 we sought to equip *P. thermoglucosidasius* DSM 2542 with the typical XylFGH transporter within the species by introducing it via plasmid-based expression. In addition, we also generated strains in which we constitutively expressed the native xylose assimilation operon *xylAB* by introducing plasmid-based expression, too. Specifically, to construct the *xylAB* overexpression plasmid, the respective coding sequence was amplified directly from the genome of *P. thermoglucosidasius* DSM 2542, whereas the coding sequence of *xylFGH* was amplified from the T-61 isolate, which was previously isolated by Daas et al., (2016) and possesses exactly the same transporter as the one present in TNO-09.020 and BH4.1 (Fig. 2). With the intention of using these operons for studies on mixed sugars we first investigated how their native promoters are regulated in the presence of glucose and xylose (Fig. 2). An *in silico* analysis of the *xylAB* and *xylFGH* promoter sequences revealed distinct differences in the location of *cre* elements. In *xylAB*, a *cre* element is identified between the transcription start site and the start codon. By contrast, *xylFGH* lacks a *cre* sequence in its promoter region, but rather contains a *cre* site within the first 100 nucleotides of the coding sequence. A similar arrangement was described by Wang et al., (2024) for the ABC transporter encoded from AOT_11435 - AOT_11445. To gain more insights on how *xylFGH* operon is regulated, the *xylFGH* promoter sequence was placed upstream of an *sfGFP* gene and cloned in pUCG3.8 plasmid vector. Additionally, we used the promoter of *xylAB* (including the *cre* sequence), which was also investigated by Wang et al., (2024) as a control for our promoter regulation investigation. Transformants carrying the plasmids were grown in microplate reader with constant monitoring of optical density and sfGFP fluorescence.

In our studies, glucose repressed sfGFP expression from the *xylAB* promoter (P_{xylAB}) both alone and in combination with xylose, likely because P_{xylAB} harbors a *cre* site (Fig. 2), indicating that CcpA binds this sequence and mediates carbon catabolite repression as also indicated by Wang et al., (2024). By contrast, sfGFP expression driven by P_{xylFGH} was only fully absent on glucose while activity was

observed on the glucose-xylose mixture. This observation is in alignment with the absence of a *cre* site in the *xylFGH* promoter region. With xylose as the only carbon source, both promoters were induced, and P_{xylFGH} showed higher maximum activity than P_{xylAB}. P_{xylAB}-driven expression was also saturated at lower xylose concentrations than P_{xylFGH}. Notably, P_{xylFGH} functions as a glucose-insensitive, xylose-inducible promoter, like the engineered P_{xylAB} variant described by Wang et al. (2024).

To allow constitutive expression independent of xylose's presence, and mitigate CCR by glucose, we replaced the native regulatory regions of *xylAB* and *xylFGH* with the P_{ldhL} promoter combined with the strong ribosome binding site of *pheB*. Thus, three strains were generated: P_{ldhL}-*xylAB*, P_{ldhL}-*xylFGH* (*cre*$^{+}$), which carries an intact *cre* sequence at the start of the *xylF* gene, and P_{ldhL}-*xylFGH*, in which the *cre* sequence was modified. To assess the two *xylFGH*-overexpressing strains (with or without *cre*), we initially cultivated them aerobically in the presence of glucose and xylose, which resulted in notable physiological differences as P_{ldhL}-*xylFGH* (*cre*$^{-}$) consumed xylose after glucose depletion faster than both the WT and P_{ldhL}-*xylFGH* (*cre*$^{+}$) (Figure S2). It also attained higher optical densities after 24 h suggesting that P_{ldhL}-*xylFGH* may present a more suitable strain for use in mixed-sugar fermentations. Next, we compared P_{ldhL}-*xylFGH*, with P_{ldhL}-*xylAB* and the WT strain in minimal medium containing xylose as the sole carbon source to assess the effect of operon overexpression. Both P_{ldhL}-*xylFGH* and P_{ldhL}-*xylAB* exhibited higher growth rates (Fig. 3) compared to WT, and evidently improved xylose consumption aerobically.

ptsG R452C and Δ rbsR mutations reduce CCR and affect the levels of proteins in glycolysis, the glucose PTS system and multiple secondary sugar operons

The reverse engineered mutants *ptsG*R452C, Δ*rbsR, ptsG*R452C Δ*rbsR* as well as P_{ldhL}-*xylAB* and P_{ldhL}-*xylFGH* overexpressing strains were assessed for sugar consumption in minimal media supplemented with glucose and xylose. Initial experiments that were conducted in aerobic conditions indicated that mutants displayed a (partial) CCR phenotype prioritizing glucose consumption over xylose (Figure S2). Yet, in tubes with reduced headspace to mimic oxygen-limiting conditions, which were previously also used in ALE (Liang et al., 2022[b]), the reverse engineered mutants showed a co-consumption phenotype (Figure S2). On the contrary, P_{ldhL}-*xylAB* consumed slightly more xylose than P_{ldhL}-*xylFGH* and WT, though for both of these strains there is hardly any co-consumption observed, emphasizing that only the reverse-engineered mutations led to a co-consumption phenotype under microaerobic conditions. Generally, the low-sugar consumption observed here was because of growth stall caused by a significant drop in pH because of accumulating acids in tube cultivations. These results were our first indication of potential CCR alleviation in reverse engineered mutants. Following this observation, we aimed to gain more insights and decipher the impact of these mutations by analyzing the associated proteomes to detect differences in protein abundances using mass spectrometry-based proteomics.

First, we compared the relative abundances of the major proteins associated with the CCR cascade across all mutants relative to the WT strain (Fig. 4). Specifically, protein levels of components of the

glucose-PTS system exhibited altered levels, particularly in the presence of Δ*rbsR* mutation (Fig. 4A). Moreover, the Δ*rbsR* mutation was associated with reduced levels of all the glucose-PTS enzymes; including PtsG, EI enzyme and HPr, which are all expressed by the same operon. In *B. subtilis*, the glucose-PTS operon is autoregulated by PtsG (Stülke et al., 1997). When phosphorylated, PtsG can act as a kinase that phosphorylates the antiterminator protein GlcT of the *ptsGHI* operon, thereby inactivating it and terminating operon transcription. This mechanism could explain the reduced abundance of PtsG, EI enzyme and HPr observed in Δ*rbsR*, if glucose uptake was impaired, leading to increased levels of phosphorylated PtsG, and consequently stronger repression of the *ptsGHI* operon. Aligned with this hypothesis, we also observed a reduced maximum specific growth rate of Δ*rbsR* on glucose (Fig. 1). Similarly, the *rbsR* deletion was related to reduced levels of almost all enzymes in the EMP glycolysis (Figure S3) and particularly Pgk, Tpi, Pgm, and Eno. In *B. subtilis* these are all transcribed from the same operon in a tetracistronic transcript (Ludwig et al., 2001), and their expression is indirectly regulated by FBP levels (Fujita et al. 2009). At high concentrations of FBP, the CggR regulator of the *gapA pgk tpi pgm eno* operon dissociates from the operator sequence allowing transcription, therefore the reduced expression observed here may be indicative of lower FBP intracellular levels. Collectively, these observations are consistent with a reduced glycolytic flux, which may be associated with the partial CCR alleviation of Δ*rbsR*. Although both *ptsG*R452C and Δ*rbsR* co-consumed glucose and xylose, no major changes were detected in the levels of *ptsGHI*-encoded proteins or glycolytic enzymes in the *ptsG*R452C mutant (Fig. 4A), suggesting that *ptsG*R452C potentially worked via a different mechanism to allow co-consumption of glucose and xylose. Indeed, a Principal Component Analysis (PCA) (Figure S4) revealed distinct variance of the protein abundances in the *ptsG*R452C and Δ*rbsR* implying that these mutations affected cellular physiology via different mechanisms despite both resulting in relief of CCR as discussed earlier.

Next, we looked into how the mutations in *ptsG* and *rbsR* affected several typically glucose-repressed operons such as the ones associated with the catabolism of xylose, ribose, arabinose and cellobiose. The enzymes and ABC transporters associated with these operons were significantly upregulated in all mutants suggesting CCR alleviation (Fig. 4B). Specifically, the extracellular binding proteins of the ribose ABC transporter, arabinose ABC transporter and the main xylose ABC transporter in DSM 2542 (Wang et al., 2024) were strongly upregulated in all mutants potentially enabling multiple entry points for xylose uptake. Intracellularly, most enzymes of the secondary sugar operons were highly upregulated with cases like the RbsD and RbsK reaching around 200 times higher abundance in the reverse engineered mutants compared to the WT. Notably, XylA and XylB, which constitute the xylose assimilation enzymes were the least impacted of all intracellular enzymes, yet their concentration levels were already considerably high (Figure S5) compared to the enzymes encoded by the ribose, arabinose and cellobiose operon. Interestingly, the R452C mutation in the PtsG was associated with almost 150 times higher expression of the EIIB component of the cellobiose PTS component suggesting an effect of this glucose-PTS mutation on another PTS system. This could possibly be attributed to a cumulative effect of both reduced CcpA-mediated repression and higher CelR (cellobiose operon regulator) activation, which is known to be activated by Hpr-Ser-46P like CcpA (Zeng and Burne, 2010).

ptsG R452C, Δ rbsR and xylAB overexpression increased lactate titers and yield

The reverse engineered *ptsG*R452C, Δ*rbsR* and *ptsG*R452C Δ*rbsR* exhibited reduced CCR, a desirable trait in mixed-sugar fermentations. Glucose and xylose metabolisms are inherently different and *P. thermoglucosidasius* WT achieves high growth rates on glucose (0.27 h^{-1}) yet significantly slows down (0.15 h^{-1}) on xylose as expected (Fig. 1). In mixed-sugar fermentations, this difference can split the fermentation into two parts, a fast-growing glucose phase that leads to high lactate titers followed by a slow-growing xylose phase compromising growth-coupled lactate productivity. To gain a better understanding on whether this is true in *P. thermoglucosidasius*, we evaluated the reverse engineered mutants as well as the xylose uptake and xylose assimilation overexpression strains in fermenter cultivations composed of 1 L working volume with microaerobic conditions (Fig. 5). Mutants *ptsG*R452C, Δ*rbsR*, *ptsG*R452C Δ*rbsR* consumed glucose and xylose simultaneously as expected, yet with notable differences between them. Specifically, *ptsG*R452C consumed glucose and xylose at a similar rate. Compared to the wild-type, this strain showed reduced glucose uptake rate and increased xylose uptake rate. Δ*rbsR* was a slow-growing strain that enabled xylose consumption in the presence of glucose. The consumption rates of both glucose and xylose were lower than what was observed in the WT, but still glucose was consumed slightly faster than xylose. This strain had consumed less sugars overall than all other mutants after 96 hours of cultivation. On the other hand, *ptsG*R452C Δ*rbsR* showed a completely reversed sugar preference as xylose consumption was prioritized over glucose. On the contrary, the *xylAB* and *xylFGH* overexpressing strains did not alleviate CCR, aligning with the results from the microaerobic tube fermentations. Still overexpression of XylAB from the *ldhL* promoter resulted in almost full xylose consumption after glucose was depleted, also resulting in the highest achieved biomass of all mutants.

Lactate titers and yields (mol-%) relative to the maximum theoretical yield were the highest in *ptsG*R452C (12.49 g/L, 65.33 mol-%), Δ*rbsR* (11.52 g/L, 72.76 mol-%) and P_{ldhL}-*xylAB* (12.05 g/L, 63.55 mol-%) (Table 3), compared to 9.26 g/L and 56.76 (mol-%) of lactate measured in WT. When comparing the total consumption of sugars, WT, *ptsG*R452C, and P_{ldhL}-*xylAB* were the best-performing strains exhibiting comparable consumption of the total sugars provided (Table 3), whereas Δ*rbsR* and *ptsG*R452C Δ*rbsR* consumed the least with the highest amount of remaining sugars in the fermentation experiment. Yet, Δ*rbsR* produced among the highest titers resulting in the best yield (72.76 mol-%) as it diverted most of the sugars to lactate. All *P. thermoglucosidasius* strains generated significant amounts of formate, acetate and ethanol in the fermenter cultivations (Table 3, Figure S7). Specifically, all reverse-engineered mutants displayed similar to WT final titers of ethanol. On the other hand, formate titers at the end of the cultivations were lower than WT, whereas acetate titers were similar between WT and *ptsG*R452C, but lower in Δ*rbsR and ptsG*R452C Δ*rbsR.* Additionally, WT and P_{ldhL}-*xylAB* exhibited similar final titers and productivity of ethanol, formate and acetate. In P_{ldhL}-*xylFGH* fermenter cultivations, we detected similar to WT ethanol levels, yet less formate and acetate particularly during the xylose-consuming phase, which aligned with the reduced xylose consumption of this strain. The accumulation of fermentation by-

products as well as potential losses from CO_2 formation limited lactate yields, yet we observed increased titers and yields in multiple strains compared to WT.

Table 3
– Summary of sugar consumption, lactate titers and yields from the batch bioreactor fermentations.

Category	**WT**	***ptsG*R452C**	**Δ*rbsR***	***ptsG*R452C Δ*rbsR***	**P_{ldhL}-*xylFGH***	**P_{ldhL}-*xylAB***
Glucose consumed (g)	9.26	8.73	8.05	4.78	8.98	8.83
Xylose consumed (g)	7.49	7.87	5.11	7.31	6.14	7.67
Total sugars consumed (g)	16.75	16.60	13.16	12.09	15.13	16.51
Final lactate titer (g/L)	9.78	12.49	11.53	9.13	9.93	11.63
Yield (moles/moles)*	1.03	1.19	1.35	1.07	1.11	1.16
Yield (mol-%)*	56.76	65.33	72.76	60.09	59.76	63.55
Final formate titer (g/L)	0.91	0.46	0.36	0.26	0.42	0.90
Final acetate titer (g/L)	0.49	0.53	0.24	0.17	0.51	0.50
Final ethanol titer (g/L)	0.64	0.62	0.60	0.61	0.64	0.66
*Equations for calculations are shown in Materials and Methods.						

DISCUSSION

Mixed-sugar microbial fermentations are often limited by CCR, a phenomenon that allows microbes to prioritize the consumption of their preferred substrate in the presence of multiple energy sources, yet this is undesired in bioproduction processes as it can compromise productivity and product titers. In this study, we focused on *P. thermoglucosidasius* by developing reverse-engineered mutants based on a previous ALE work (Liang et al., 2022[b]), which enabled co-consumption of glucose and xylose. Additionally, we equipped *P. thermoglucosidasius* DSM 2542 with constitutive expression of its native xylose assimilation pathway (*xylAB*) and a xylose ABC transporter operon (*xylFGH*) encoded in *P. thermoglucosidasius* T-61. All reverse engineered mutant strains when tested in microaerobic conditions showed improved co-consumption of xylose consumption in the presence of glucose, and analysis of their proteome revealed that multiple operons regulated by CCR were significantly upregulated confirming that mutating the *ptsG* and knocking out the *rbsR* can impact intracellular processes, which impose the hierarchical consumption of sugars in *P. thermoglucosidasius.* In the fermentations of all reverse engineered mutant strains, glucose consumption was slowed down, indicating that this may be a

critical factor to enable xylose consumption in mixed-sugar fermentations. Reduced glucose consumption in fermentations with simultaneous consumption of glucose-xylose has also been observed in other studies in *E. coli* strains (Kaplan et al., 2024)d *subtilis* (Zhang et al., 2016).

In our studies, the reduced glucose consumption displayed by *ptsG*R452C may be attributed to the role of PtsG since it actively participates in the import and phosphorylation of glucose, and perhaps the introduced mutation affected the uptake and/or phosphorylation rate of the sugar as suggested in previous investigations that involved PtsG (Kim et al., 2015), yet we did not see an effect on the expression levels of the glucose PTS system, which was more obvious in the Δ*rbsR* strain. Alternatively, the mutation in PtsG may also have contributed to making the glucose-PTS system consuming xylose better. In fact, *ptsG* removal in a strain of *Corynebacterium glutamicum* (Wang et al., 2014) abolished growth on xylose, whereas *ptsG* complementation in Δ*ptsG* restored growth on xylose suggesting that *ptsG* may also play an active role in xylose importation. Similarly, an *E. coli* Δ*ptsG* (Dev et al., 2022) and a *Klebsiella oxytoca* strain carrying a spontaneous *ptsG* mutation allowed simultaneous consumption of glucose and xylose (Phosriran et al., 2026) highlighting a glucose-PTS potential role in xylose utilization. Furthermore, in our microplate reader experiments under aerobic conditions (Fig. 1), *ptsG*R452C exhibited a significantly higher growth rate in xylose-containing media further supporting the hypothesis that the mutated glucose-PTS system may play a role in xylose utilization in *P. thermoglucosidasius*, and potentially could explain the improved co-consumption observed in our experiments. This also likely explains why this mutation does not result in a strong decrease in PtsG levels during growth on a glucose-xylose mixture. While glucose import via the PTS is reduced, increased xylose consumption may help maintain lower PtsG phosphorylation levels, thereby sustaining its expression. Once inside the cell, xylose can be metabolized by XylA and XylB that show rather high expression in the wild-type and limited induction in the PtsG mutant strain (Fig. 4, S6).

Regarding the Δ*rbsR* strain, growth on glucose was impaired in both aerobic microplate cultivations (Fig. 1) and fermenter cultivations (Fig. 5). In mixed-sugar fermentations, Δ*rbsR* was also the slowest-growing strain, consumed the lowest amount of total sugars after 96 h, and reached the lowest maximum OD_{600} among all mutants tested. Together, these observations suggest that reduced glucose consumption is a central consequence of *rbsR* deletion and may explain the partial alleviation of CCR observed in this mutant. However, the mechanism by which *rbsR* deletion reduces glucose consumption remains unclear.

Proteome analysis supports the idea that glucose uptake through the PTS is impaired in Δ*rbsR*. The mutant exhibited reduced abundance of PtsG, EI, and HPr, which are encoded by the same glucose-induced operon and are negatively regulated by phosphorylated PtsG. This pattern is consistent with a scenario in which glucose uptake is reduced, leading to increased levels of phosphorylated PtsG and consequently lower expression of the glucose PTS operon. In parallel, several glycolytic enzymes were also downregulated, including Tpi, Pgk, Pgm, and Eno (Figure S3). Because these enzymes are expressed from the CggR-regulated *gapA-pgk-tpi-pgm-eno* operon, their reduced abundance may indicate lower intracellular FBP levels in Δ*rbsR*. This would be consistent with reduced glycolytic flux rather than

representing an independent mechanism. The upstream cause of this reduced glucose uptake remains unresolved. One possibility is that derepression of ribose, xylose, and arabinose ABC transporters in Δ*rbsR* interferes with glucose uptake more directly. For example, increased expression of these transporters as observed in Δ*rbsR* could compete for sugar binding or uptake. A second possibility is that strong overexpression of multiple ABC transporters increases membrane crowding, thereby reducing the effective incorporation or abundance of PtsG in the membrane.

Lastly, it cannot be excluded that the altered protein synthesis demands in the Δ*rbsR* mutant, driven by the increased expression of ribose, arabinose, and xylose metabolic enzymes as well as ABC transporters, reshaped central metabolic fluxes and indirectly reduced PEP availability. Enhanced anabolic activity may have redirected carbon flux toward biosynthetic pathways such as the shikimate pathway (aromatic amino acid synthesis), which relies on PEP as a precursor. This redistribution of metabolic flux could have limited the pool of PEP available for glucose PTS-mediated phosphorylation, thereby slowing glucose uptake. Additionally, Δ*rbsR* was a slow-growing mutant and displayed the highest lactate yields in fermentation experiments, diverting approximately 72% of the consumed sugars toward lactate production, more than any other mutant analyzed. This phenotype is indicative of altered redox and energetic balances, which may have further constrained central carbon metabolism and potentially have indirectly contributed to reduced PEP availability for PTS-mediated glucose uptake.

In addition to these uptake-related explanations, a more direct role of RbsR in CCR regulation cannot be excluded. In *B. subtilis*, RbsR has been reported to interact with HPr-Ser46-P (Müller et al., 2006), forming a complex with some structural similarity to CcpA–HPr-Ser46-P. Although the relevance of this mechanism in *P. thermoglucosidasius* remains unknown, it raises the possibility that *rbsR* deletion may affect CCR not only indirectly through reduced glucose uptake, but also through altered regulatory interactions. Overall, the available data support a model in which *rbsR* deletion lowers glucose uptake and glycolytic flux, and that this reduction in glucose catabolism contributes to partial CCR alleviation. The precise reason for the initial reduction in glucose uptake, however, remains to be determined. To further elucidate the underlying mechanisms, future studies should focus on quantifying PEP levels, given its central role in PTS-mediated glucose uptake and its influence on the phosphorylation state of the glucose-PTS system, FBP concentrations, and downstream carbon catabolite repression signaling.

As for the double mutant *ptsG*R452C Δ*rbsR*, our findings suggested a completely reversed hierarchy regarding the sugar preference as xylose was preferred over glucose. *ptsG*R452C exhibited approximately equal glucose and xylose consumption (Fig. 5). The combined presence of the Δ*rbsR* mutation associated with decreased abundance of glucose PTS components (Fig. 4) and glycolytic enzymes (Figure S3), and the *ptsG*R452C mutation, which reduced carbon catabolite repression and increased xylose consumption (Fig. 1,4), may have collectively altered sugar utilization patterns yielding a strain with reduced glucose consumption and enhanced xylose uptake, resulting in an unusual preference for xylose relative to glucose. To further support this, *ptsG*R452C overexpressing *xylAB* and *xylFGH* also led to a similar phenotype to *ptsG*R452C Δ*rbsR* preferring xylose over glucose (Figure S8).

As shown in this study and by Wang et al., (2024) xylose uptake and assimilation operons are induced effectively by xylose. However, during active growth on xylose, progressively decreasing extracellular xylose concentrations may affect both the expression of the XylA, XylB enzymes and xylose ABC transporter, as well as possibly impact the kinetics of xylose importation and assimilation. In our studies, we proposed that overexpression of *xylAB* and *xylFGH* can lead to higher growth rates under aerobic conditions in xylose-containing media. Yet, only *xylAB* overexpression was beneficial in mixed-sugar fermentation that led to higher biomass and lactate titers, when cells were consuming xylose after glucose depletion. Increased lactate titers and yields were also observed in the fermenter cultivations of *ptsG*R452C and Δ*rbsR* mutant strains, confirming how reduced CCR can be beneficial in sugar-mixed bioproduction processes. Yet, these mutations were associated with slower sugar consumption rates, particularly for glucose. In the fermenter cultivations of *ptsG*R452C and Δ*rbsR* reduced levels of formate and both formate and acetate were detected, respectively. However, ethanol titers were similar to the ones measured in WT cultivations, suggesting that knocking-out the pathway for ethanol production may be an effective approach to increase lactate yields on substrate as also done in previous investigations by Liu et al., (2024). Future studies may focus on using mutants as the ones described here as platforms to completely eliminate competing fermentation pathways, as well as to optimize the fermentation process, which have both been shown to be effective approaches in increasing lactate titers and yields (Abdel-Rahman et al., 2021).

CONCLUSIONS

P. thermoglucosidasius DSM 2542 is a promising microbial platform for implementation in bio-based production processes using second-generation feedstocks. Here, inspired by a previous ALE investigation, we constructed multiple strains able to co-consume glucose and xylose under microaerobic conditions. Analysis on the proteome level revealed distinct differences in how CCR was reduced in different mutants. Additionally, we derepressed and overexpressed the native xylose assimilation pathway and a xylose ABC transporter from a related strain, which resulted in higher growth rates aerobically. Multiple of our strains outperformed the WT both in final lactate titers and fermentation yields.

DATA AVAILABILITY

The datasets supporting the conclusions of this article are included within the article (and its additional files). Additionally, mass spectrometric raw files, the DIA-NN output files as well as the protein fasta file are available in the ProteomeXchange Consortium via the PRIDE partner repository and can be accessed using the identifier PXD080214 (https://proteomecentral.proteomexchange.org/cgi/GetDataset?ID=PXD080214). Access to the data can be obtained by logging in via **PRIDE Archive login page** https://www.ebi.ac.uk/pride/login using the following credentials under the “Login using Reviewer Token” section: Project accession: PXD080214; Token: kOz28P9Gz0gg).

Declarations

SUPPLEMENTARY DATA

Supplementary Data are available as a separate file.

CONFLICT OF INTEREST

The authors declare no competing financial interest. P.K. and H.J.R. are employed by the commercial company Corbion (Gorinchem, The Netherlands).

FUNDING

DECLARATION

This work was supported by the Talent4BBI; a Marie Skłodowska-Curie COFUND project managed by BiOrbic, the SFI Research Centre in Ireland. Talent4BBI project received funding from EU Horizon 2020 research and innovation program under grant agreement N0. 101034323. This funding was awarded to PK. The funder had no role in study design, data collection and analysis, decision to publish, or preparation of the manuscript.

Author Contribution

P.K.: Conceptualization, Methodology, Data curation, Formal analysis, Investigation, Project Administration, Resources, Validation, Visualization, Writing – original draft. M.M: Data curation, Investigation, Resources. J.d.V.: Investigation, Resources. C.L.: Supervision, Project administration, Conceptualization, Writing – review & editing. H.J.R.: Supervision, Writing – review & editing, Funding acquisition. N.J.C & R.v.K.: Supervision, Writing – review & editing, Project administration, Funding acquisition.

Acknowledgement

PK acknowledges funding from Talent4BBI; a Marie Skłodowska-Curie COFUND project managed by BiOrbic, the SFI Research Centre in Ireland. Talent4BBI project received funding from the EU Horizon 2020 research and innovation program under the grant agreement No. 101034323. The authors thank Franziska Hackbarth for her excellent technical assistance and maintenance of mass spectrometers.

Data Availability

The datasets supporting the conclusions of this article are included within the article (and its additional files). Additionally, mass spectrometric raw files, the DIA-NN output files as well as the protein fasta file are available in the ProteomeXchange Consortium via the PRIDE partner repository and can be accessed using the identifier PXD080214(https://proteomecentral.proteomexchange.org/cgi/GetDataset?ID=PXD080214; Project accession: PXD080214; Token: kOz28P9Gz0gg).

References

1. Abdel-Rahman MA, Hassan SE-D, Alrefaey HMA, Elsakhawy T. (2021). Efficient co-utilization of biomass-derived mixed sugars for lactic acid production by Bacillus coagulans Azu-10. Fermentation, 7(1), 28. https://doi.org/10.3390/fermentation7010028
2. Abele M, Doll E, Bayer FP, Meng C, Lomp N, Neuhaus K, Scherer S, Kuster B, Ludwig C. (2023). Unified workflow for the rapid and in-depth characterization of bacterial proteomes. Molecular & Cellular Proteomics, 22(8), 100612. https://doi.org/10.1016/j.mcpro.2023.100612
3. Álvarez C, Reyes-Sosa FM, Díez B. (2016). Enzymatic hydrolysis of biomass from wood. Microbial Biotechnology, 9(2), 149–56. https://doi.org/10.1111/1751-7915.12346
4. Bartosiak-Jentys J, Hussein AH, Lewis CJ, Leak DJ. (2013). Modular system for assessment of glycosyl hydrolase secretion in Geobacillus thermoglucosidasius. Microbiology, 159, 1267–75. https://doi.org/10.1099/mic.0.066332-0
5. Bidart GN, Gharabli H, Welner DH. (2023). Functional characterization of the phosphotransferase system in Parageobacillus thermoglucosidasius. Scientific Reports, 13, 7131. https://doi.org/10.1038/s41598-023-33918-1
6. Broda M, Yelle DJ, Serwanska K. (2022). Bioethanol production from lignocellulosic biomass—Challenges and solutions. Molecules, 27(24), 8717. https://doi.org/10.3390/molecules27248717
7. Calverley J, Ibenegbu C, Hussein-Sheik A, Bandulasena H, H. C., Leak DJ. (2024). Ethanologenic fermentation by Parageobacillus thermoglucosidasius with continuous hot microbubble gas-stripping. Microbial Cell Factories, 23, 165. https://doi.org/10.1186/s12934-024-02433-x
8. Cripps RE, Eley K, Leak DJ, Rudd B, Taylor M, Todd M, Boakes S, Martin S, Atkinson T. (2009). Metabolic engineering of Geobacillus thermoglucosidasius for high yield ethanol production. Metabolic Engineering, 11(6), 398–408. https://doi.org/10.1016/j.ymben.2009.08.005
9. Cunha JT, Soares PO, Baptista SL, Costa CE, Domingues L. (2020). Engineered Saccharomyces cerevisiae for lignocellulosic valorization: A review and perspectives on bioethanol production. Bioengineered, 11(1), 883–903. https://doi.org/10.1080/21655979.2020.1801178
10. Daas MJA, van de Weijer AHP, de Vos WM, van der Oost J, van Kranenburg R. (2016). Isolation of a genetically accessible thermophilic xylan degrading bacterium from compost. Biotechnology for Biofuels, 9, 210. https://doi.org/10.1186/s13068-016-0618-7
11. Demichev V, Messner CB, Vernardis SI, Lilley KS, Ralser M. (2020). DIA-NN: neural networks and interference correction enable deep proteome coverage in high throughput. Nat Methods 17, 41–4. https://doi.org/10.1038/s41592-019-0638-x

12. Dev C, Jilani SB, Yazdani SS. (2022). Adaptation on xylose improves glucose–xylose co-utilization and ethanol production in a carbon catabolite repression (CCR) compromised ethanologenic strain. Microbial Cell Factories, 21, 154. https://doi.org/10.1186/s12934-022-01879-1
13. Devi A, Bajar S, Kour H, Kothari R, Pant D, Singh A. (2022). Lignocellulosic biomass valorization for bioethanol production: A circular bioeconomy approach. BioEnergy Research, 15, 1820–41. https://doi.org/10.1007/s12155-022-10401-9
14. Doellinger J, Schneider A, Hoeller M, Lasch P. (2020). Sample preparation by easy extraction and digestion (SPEED) - a universal, rapid, and detergent-free protocol for proteomics based on acid extraction. Molecular & Cellular Proteomics, 19(1), 209–22. https://doi.org/10.1074/mcp.TIR119.001616
15. Francois JM, Alkim C, Morin N. (2020). Engineering microbial pathways for production of bio-based chemicals from lignocellulosic sugars: Current status and perspectives. Biotechnology for Biofuels, 13, 118. https://doi.org/10.1186/s13068-020-01744-6
16. Frenzel E, Legebeke J, van Stralen A, van Kranenburg R, Kuipers OP. (2018). In vivo selection of sfGFP variants with improved and reliable functionality in industrially important thermophilic bacteria. Biotechnology for biofuels, 11, 8. https://doi.org/10.1186/s13068-017-1008-5
17. Fujita Y. (2009). Carbon catabolite control of the metabolic network in Bacillus subtilis. Bioscience, Biotechnology, and Biochemistry, 73(2), 245–59. https://doi.org/10.1271/bbb.80479
18. Galinier A, Haiech J, Kilhoffer MC, Jaquinod M, Stülke J, Deutscher J, Martin-Verstraete I. (1997). The Bacillus subtilis crh gene encodes a HPr-like protein involved in carbon catabolite repression. Proceedings of the National Academy of Sciences of the United States of America, 94(16), 8439–44. https://doi.org/10.1073/pnas.94.16.8439
19. Gerault MA, Camoin L, Granjeaud S. (2024). DIAgui: a Shiny application to process the output from DIA-NN. Bioinformatics advances, 4(1), vbae001. https://doi.org/10.1093/bioadv/vbae001
20. Gonzalez JE, Long CP, Antoniewicz MR. (2017). Comprehensive analysis of glucose and xylose metabolism in Escherichia coli under aerobic and anaerobic conditions by 13C metabolic flux analysis. Metabolic Engineering, 39, 9–18. https://doi.org/10.1016/j.ymben.2016.11.003
21. Görke B, Stülke J. (2008). Carbon catabolite repression in bacteria: Many ways to make the most out of nutrients. Nature Reviews Microbiology, 6(8), 613–24. https://doi.org/10.1038/nrmicro1932
22. Hill J. (2022). The sobering truth about corn ethanol. Proceedings of the National Academy of Sciences of the United States of America, 119(11), e2200997119. https://doi.org/10.1073/pnas.2200997119
23. Hussein AH, Lisowska BK, Leak DJ. (2015). The genus Geobacillus and their biotechnological potential. Advances in Applied Microbiology, 92, 1–48. https://doi.org/10.1016/bs.aambs.2015.03.001
24. Ibrahim MF, Ramli N, Bahrin EK, Abd-Aziz S. (2017). Cellulosic biobutanol by Clostridia: Challenges and improvements. Renewable and Sustainable Energy Reviews, 79, 1241–54. https://doi.org/10.1016/j.rser.2017.05.184

25. Kaplan NA, Islam KN, Kanis FC, Verderber JR, Wang X, Jones JA, Koffas MAG. (2024). Simultaneous glucose and xylose utilization by an Escherichia coli catabolite repression mutant. Applied and Environmental Microbiology, 90(5), e02169–23. https://doi.org/10.1128/aem.02169-23
26. Kim JH, Block DE, Mills DA. (2010). Simultaneous consumption of pentose and hexose sugars: An optimal microbial phenotype for efficient fermentation of lignocellulosic biomass. Applied Microbiology and Biotechnology, 88(5), 1077–85. https://doi.org/10.1007/s00253-010-2839-1
27. Kim SM, Choi BY, Ryu YS, Jung SH, Park JM, Kim GH, Lee SK. (2015). Simultaneous utilization of glucose and xylose via novel mechanisms in engineered Escherichia coli. Metabolic engineering, 30, 141–8. https://doi.org/10.1016/j.ymben.2015.05.002
28. Landmann JJ, Busse RA, Latz J-H, Singh KD, Stülke J, Görke B. Crh, the paralogue of the phosphocarrier protein HPr, controls the methylglyoxal bypass of glycolysis in Bacillus subtilis. Mol Microbiol. 2011;82:770–87. https://doi.org/10.1111/j.1365-2958.2011.07857.x.
29. Lennartsson PR, Erlandsson P, Taherzadeh MJ. (2014). Integration of the first and second generation bioethanol processes and the importance of by-products. Bioresource Technology, 165, 3–8. https://doi.org/10.1016/j.biortech.2014.01.127
30. Liang J, Roberts A, van Kranenburg R, Bolhuis A, Leak DJ. (2022a). Relaxed control of sugar utilization in Parageobacillus thermoglucosidasius DSM 2542. Microbiological Research, 256, 126957. https://doi.org/10.1016/j.micres.2021.126957
31. Liang J, van Kranenburg R, Bolhuis A, Leak DJ. (2022b). Removing carbon catabolite repression in Parageobacillus thermoglucosidasius DSM 2542. Frontiers in Microbiology, 13, 985465. https://doi.org/10.3389/fmicb.2022.985465
32. Lin PP, Rabe KS, Takasumi JL, Kadisch M, Arnold FH, Liao JC. (2014). Isobutanol production at elevated temperatures in thermophilic Geobacillus thermoglucosidasius. Metabolic Engineering, 24, 1–8. https://doi.org/10.1016/j.ymben.2014.03.006
33. Liu J, Han X, Tao F, Xu P. (2024). Metabolic engineering of Geobacillus thermoglucosidasius for polymer-grade lactic acid production at high temperature. Bioresource Technology, 393, 130164. https://doi.org/10.1016/j.biortech.2023.130164
34. Ludwig H, Homuth G, Schmalisch M, Dyka FM, Hecker M, Stülke J. (2001). Transcription of glycolytic genes and operons in Bacillus subtilis: Evidence for the presence of multiple levels of control of the gapA operon. Molecular Microbiology, 41(2), 409–22. https://doi.org/10.1046/j.1365-2958.2001.02523.x
35. Millgaard M, Bidart GN, Pogrebnyakov I, Nielsen AT, Welner DH. (2023). An improved integrative GFP-based vector for genetic engineering of Parageobacillus thermoglucosidasius facilitates the identification of a key sporulation regulator. AMB Express, 13(1), 44. https://doi.org/10.1186/s13568-023-01544-9
36. Mohr A, Raman S. (2013). Lessons from first generation biofuels and implications for the sustainability appraisal of second generation biofuels. Energy Policy, 63, 114–22. https://doi.org/10.1016/j.enpol.2013.08.033

37. Müller W, Horstmann N, Hillen W, Sticht H. (2006). The transcription regulator RbsR represents a novel interaction partner of the phosphoprotein HPr-Ser46-P in Bacillus subtilis. The FEBS Journal, 273(6), 1251–61. https://doi.org/10.1111/j.1742-4658.2006.05148.x
38. Olofsson K, Bertilsson M, Lidén G. (2008). A short review on SSF - An interesting process option for ethanol production from lignocellulosic feedstocks. Biotechnology for Biofuels, 1, 1–14. https://doi.org/10.1186/1754-6834-1-7
39. Paredes-Barrada M, Kopsiaftis P, Claassens NJ, van Kranenburg R. (2024). Parageobacillus thermoglucosidasius as an emerging thermophilic cell factory. Metabolic Engineering, 83, 39–51. https://doi.org/10.1016/j.ymben.2024.03.001
40. Phosriran C, Gosalawit C, Suvarnakuta S, Feher C. (2026). Transcriptomic analysis of engineered and evolved Klebsiella oxytoca with efficient glucose/xylose co-utilization and succinate production. Bioresource Technology, 442, 133649. https://doi.org/10.1016/j.biortech.2025.133649
41. Rappsilber J, Mann M, Ishihama Y. (2007). Protocol for micro-purification, enrichment, pre-fractionation and storage of peptides for proteomics using StageTips. Nature Protocols, 2(8), 1896–906. https://doi.org/10.1038/nprot.2007.261
42. Singhvi MS, Gokhale DV. (2019). Lignocellulosic biomass: Hurdles and challenges in its valorization. Applied Microbiology and Biotechnology, 103(23–24), 9305–20. https://doi.org/10.1007/s00253-019-10212-7
43. Stülke J, Martin-Verstraete I, Zagorec M, Rose M, Klier A, Rapoport G. (1997). Induction of the Bacillus subtilis ptsGHI operon by glucose is controlled by a novel antiterminator, GlcT. Molecular Microbiology, 25(1), 65–78. https://doi.org/10.1046/j.1365-2958.1997.4351797.x
44. Suzuki Y, Kishigami T, Inoue K, Mizoguchi Y, Eto N, Takagi M, Abe S. (1983). Bacillus thermoglucosidasius sp. nov., a new species of obligately thermophilic bacilli. Systematic and Applied Microbiology, 4(4), 487–95. https://doi.org/10.1016/S0723-2020(83)80006-X
45. Turner P, Mamo G, Karlsson EN. (2007). Potential and utilization of thermophiles and thermostable enzymes in biorefining. Microbial Cell Factories, 6, 9. https://doi.org/10.1186/1475-2859-6-9
46. van Kranenburg R, Verhoef A, Machielsen MP. (2017). Genetic modification of (S)-lactic acid producing thermophilic bacteria. Patent EP3177741B1.
47. Vinuselvi P, Kim MK, Lee SK, Ghim CM. (2012). Rewiring carbon catabolite repression for microbial cell factory. BMB Reports, 45(2), 59–70. https://doi.org/10.5483/BMBRep.2012.45.2.59
48. Wang C, Cai H, Zhou Z, Zhang K, Chen Z, Chen Y, Wan H, Ouyang P. (2014). Investigation of ptsG gene in response to xylose utilization in Corynebacterium glutamicum. Journal of Industrial Microbiology and Biotechnology, 41(8), 1249–58. https://doi.org/10.1007/s10295-014-1455-y
49. Wang J, Li Z, Wang W, Pang S, Yao Y, Yuan F, Wang H, Xu Z, Pan G, Liu Z, Chen Y, Fan K. (2022). Dynamic control strategy to produce riboflavin with lignocellulose hydrolysate in the thermophile Geobacillus thermoglucosidasius. ACS Synthetic Biology, 11(3), 1146–56. https://doi.org/10.1021/acssynbio.2c00087

50. Wang J, Wang W, Chen Y, Liu Z, Ji X, Pan G, Li Z, Fan K. (2024). Development of a xylose-inducible and glucose-insensitive expression system for Parageobacillus thermoglucosidasius. Applied Microbiology and Biotechnology, 108(1), 493. https://doi.org/10.1007/s00253-024-13333-w
51. Yang Z, Li Z, Li B, Bu R, Tan GY, Wang Z, Yan H, Xin Z, Zhang G, Li M, Xiang H, Zhang L, Wang W. (2023). A thermostable type I-B CRISPR-Cas system for orthogonal and multiplexed genetic engineering. Nature communications, 14(1), 6193. https://doi.org/10.1038/s41467-023-41973-5
52. Yang Z, Sun Q, Tan G, Zhang Q, Wang Z, Li C, Qi F, Wang W. (2020). Engineering thermophilic Geobacillus thermoglucosidasius for riboflavin production. Microbial Biotechnology, 13(6), 1801–11. https://doi.org/10.1111/1751-7915.13543
53. Zeng L, Burne RA. (2010). Seryl-phosphorylated HPr regulates CcpA-independent carbon catabolite repression in conjunction with PTS permeases in Streptococcus mutans. Molecular Microbiology, 75(5), 1145–58. https://doi.org/10.1111/j.1365-2958.2009.07029.x
54. Zhang B, Li XL, Fu J, Li N, Wang Z, Tang YJ, Chen T. (2016). Production of acetoin through simultaneous utilization of glucose, xylose, and arabinose by engineered Bacillus subtilis. PLoS ONE, 11(7), e0159298. https://doi.org/10.1371/journal.pone.0159298

Figures

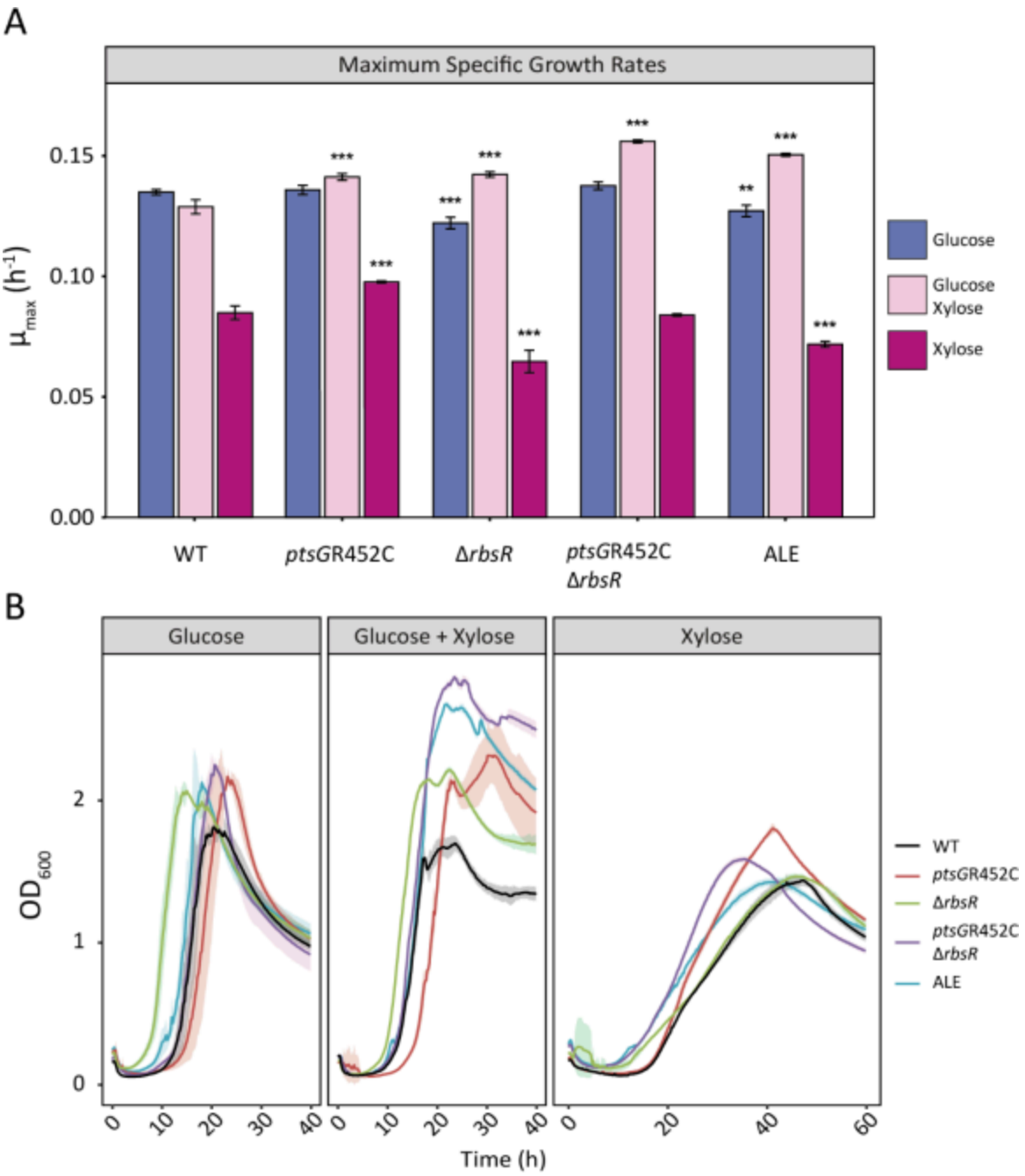


Figure 1

Aerobic growth comparison of WT, ptsGR452C, ΔrbsR, ptsGR452C ΔrbsR and ALE strains. Microplate reader experiment in TMM minimal media containing either 0.2% (w/v) glucose or 0.2% (w/v) xylose or 0.2% (w/v) glucose + 0.2 % (w/v) xylose as carbon source. Growth rates μ_{max} (h^{-1}) were calculated with the linear regression of RStudio using a time window of 100 timepoints and at least 1.5 doubling times and $R^2 > 0.8$ for the best model to fit. Tukey's Honestly Significant Difference (HSD) test was performed to determine statistically significant differences of the mutants using WT as the control. ***(3 stars): p<0.001, **(2 stars): p<0.01, *(1 star): p<0.05, no star: no statistically significant differences to the WT.

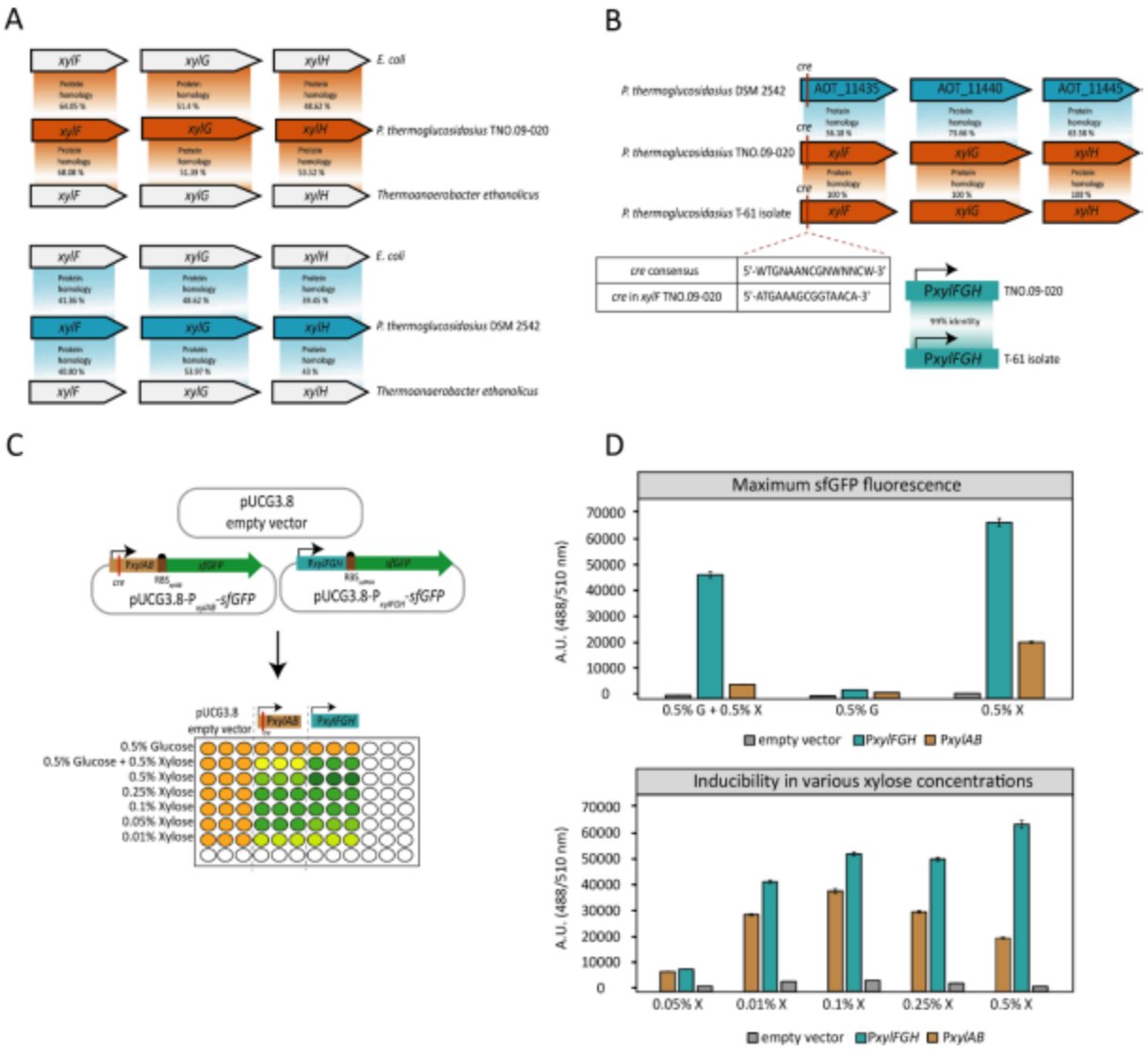


Figure 2

Selection of the *xylFGH* operon from *P. thermoglucosidasius* TNO-09.020 and *xylAB/xylFGH* promoter studies. (A) The xylose ABC transporter (XylFGH) of *P. thermoglucosidasius* TNO-09.020 and the recently identified as xylose ABC transporter in DSM 2542 were compared with the respective XylFGH from *E.coli* and *Thermoanaerobacter ethanolicus* using the Smith-Waterman local alignment. XylFGH from TNO-09.020 showed a higher homology to the control transporters compared to DSM 2542. (B) Protein and promoter homologies of xylose ABC transporter operons encoded by TNO-09.020 and DSM 2542. The *cre* sequence in the *xylFGH* of T-61 isolate was modified to avoid catabolite repression on transporter expression. Promoters of TNO-09.020 and T-61 displayed 99% similarity with their only difference being one extra nucleotide present in the promoter of TNO-09.020 (Figure S1). (C) Schematic representation of the two plasmids used to characterize the *xylFGH* and *xylAB* promoters in microplate reader. Fluorescence (488 nm excitation, 510 nm emission, Gain=80) and optical density (600 nm) were monitored for 48 hours. (D) Fluorescence signal from *P. thermoglucosidasius* DSM 2542 expressing a thermostable sfGFP variant using the native *xylAB* promoter and the TNO-09.020/T-61 *xylFGH* promoter in minimal media containing 0.5% (w/v) glucose, 0.5% (w/v) xylose, 0.5% (w/v) glucose + 0.5% (w/v)

xylose or a range of xylose concentrations 0.01% (w/v) - 0.5% (w/v). Fluorescence measurements were normalized to OD_{600} of the cultures.

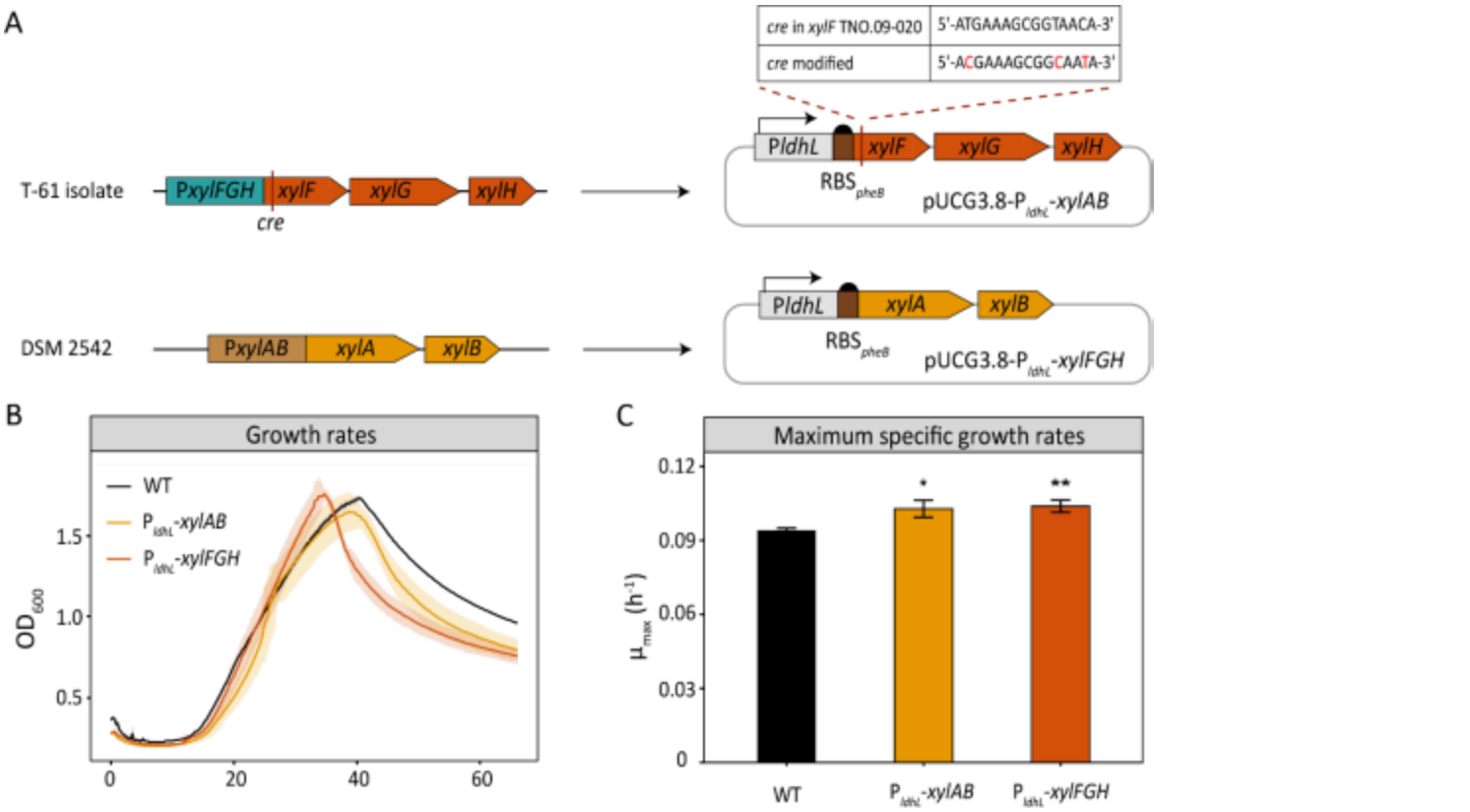


Figure 3

Overexpression of *xylAB* and *xylFGH* operons in *P. thermoglucosidasius* DSM 2542. (A) The structure of *xylFGH* and *xylAB* operons in T-61 isolate and *P. thermoglucosidasius* DSM 2542, respectively. Plasmid vectors were constructed using the P_{ldhL} promoter to drive expression of the *xylAB* and *xylFGH* operons. In the case of *xylFGH*, *cre* was modified to disrupt the consensus sequence recognized by CcpA. (B, C) Growth curves and growth rates of *P. thermoglucosidasius* DSM 2542 Δ*sigF* pUCG3.8 (WT), P_{ldhL}-*xylAB* and P_{ldhL}-*xylFGH* (without the *cre* element) in xylose-containing media. Maximum specific growth rates were calculated using the linear regression of R studio with requirements of 1.5 doubling time and a time window of 100 sampling times (approx. 1200 minutes) and $R^2 > 0.8$. Star (* or **) indicates statistically significant difference ($p_{value} < 0.05$) and ($p_{value} < 0.01$), respectively.

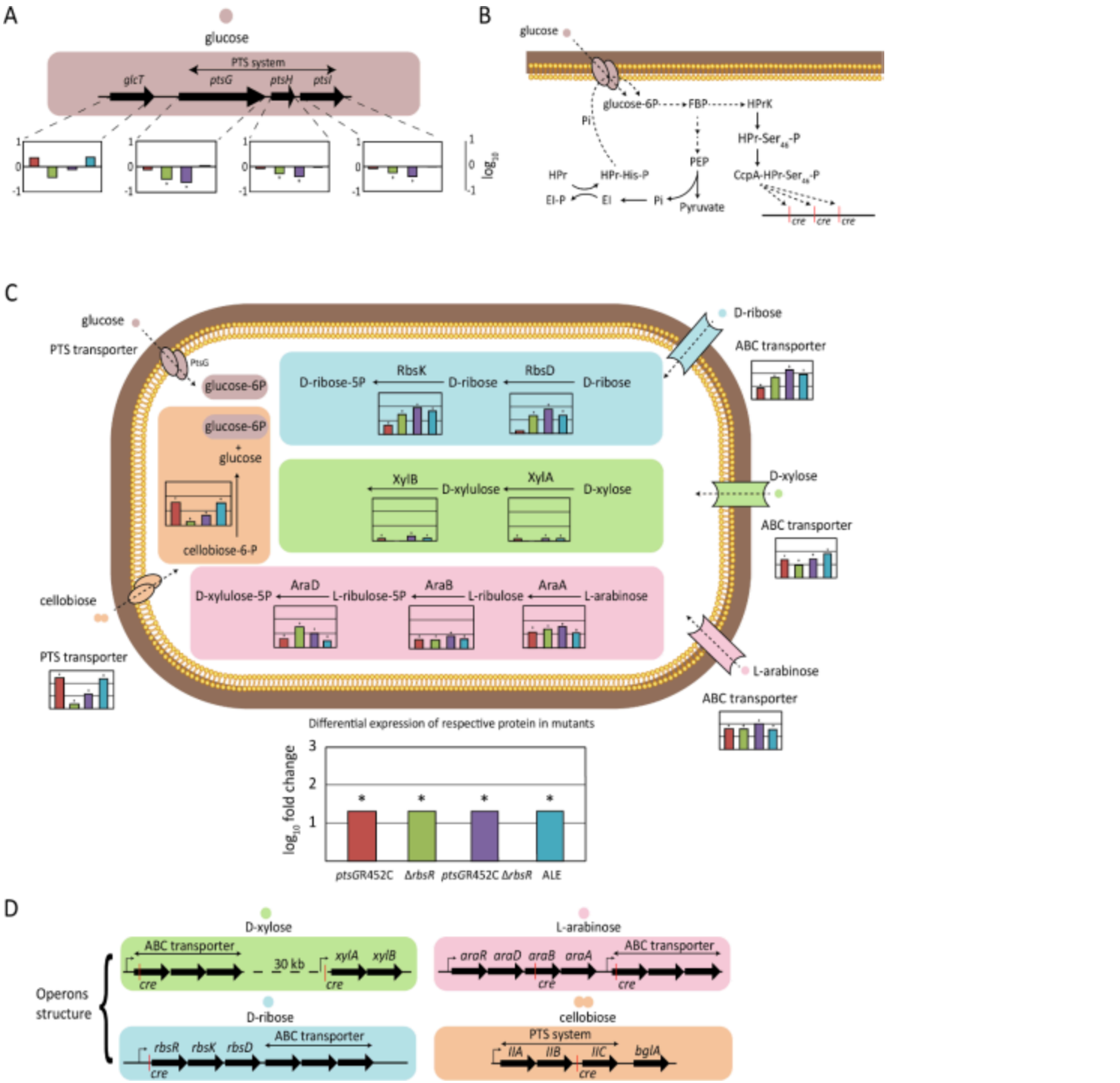


Figure 4

Differential expression of proteins from operons governed by CCR in reverse engineered mutants. WT, *ptsG*R452C, Δ*rbsR* and *ptsG*R452C Δ*rbsR* and ALE strains were cultivated in TMM media containing 1% (w/v) glucose and 1% (w/v) xylose in microaerobic conditions for 24 hours. Cell lysates were analyzed using mass spectrometry-based proteomics to detect protein expression levels. (A) Protein abundance differences across the mutants relative to the WT for proteins encoded by the *ptsGHI* operon. Values are presented on a $\log_{10}$ scale (−1 to 1) and represent the log-transformed protein abundance ratio of each mutant relative to the wild type. Each colored bar represents the $\log_{10}$ fold change in protein abundance

in the mutant (red - *ptsG*R452C, green Δ*rbsR*, purple *ptsG*R452C Δ*rbsR*, blue – ALE) relative to the wild type for the respective protein. The *ptsGHI* operon is composed of the *glcT*, *ptsG*, *ptsH* and *ptsI* genes expressing the GlcT antiterminator protein, PtsG, HPr and EI enzyme, which all comprise the glucose-PTS. (B) PtsG is the transmembrane component of glucose-PTS responsible for binding, uptaking and phosphorylating glucose, PtsI (EI) is the cytoplasmic enzyme transferring the phosphate group from PEP to HPr, which in turn passes it to the PtsG to phosphorylate glucose. (C) Differential expression levels of enzymes and extracellular binding proteins of transporters from ribose, xylose, arabinose and cellobiose operons in *P. thermoglucosidasius* DSM 2542 were determined using mass spectrometry-based proteomics. Values are presented on a $\log_{10}$ scale (0 to 3) and represent the log-transformed protein abundance ratio of each mutant relative to the WT. Pair-wise differential analyses were performed through Student t-tests. The resulting p-values were adjusted by Bonferroni using a $p_{value} < 0.0125$ (*). (D) Genomic organization of the xylose, ribose, arabinose and cellobiose operons. Genes encoding the depicted differentially expressed enzymes and transporter components are displayed along with the predicted promoters (angled arrows), and *cre* sequences (red lines).

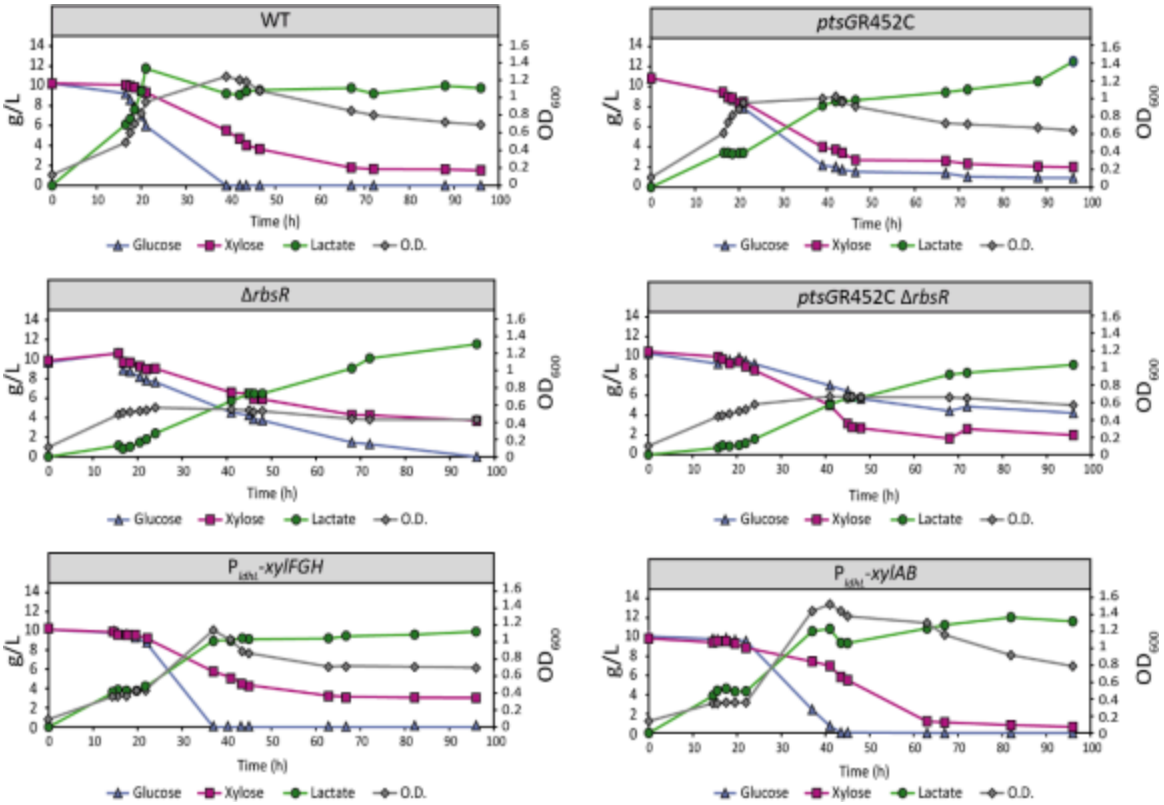


Figure 5

Bioreactor batch fermentations of reverse engineered and xylose-utilization improved mutants. All mutants were cultivated in a starting volume of 1 L TMM media supplemented with 1% (w/v) glucose and 1% (w/v) xylose. Glucose, xylose and lactate levels as well as optical density (OD_{600}) were monitored for 96 hours in each fermentation.

Supplementary Files

This is a list of supplementary files associated with this preprint. Click to download.

- Kopsiaftisetal.2026SupplementaryFile.docx
- APPENDIX.docx